

Cite this: *J. Mater. Chem. C*, 2021,
9, 4217

The effect of electron-withdrawing substituents in asymmetric anthracene derivative semiconductors†

Si Liu,^{‡a} Lei Zheng,^{‡a} Mingxi Chen,^a Yajing Sun,^a Peng Wang,^a Shuyu Li,^a
Hongnan Wu,^a Xiaotao Zhang ^{*a} and Wenping Hu ^{ab}

Three anthracene derivatives, referred to as 2-phenyl anthracene (Ph-Ant), 2-thiazole anthracene (TZ-Ant), and 2-pentafluorophenyl anthracene (F₅Ph-Ant), were designed and synthesized to reveal the effects of the electron-withdrawing substituents on the molecular packing structure and photoelectric properties of the anthracene core. As the electron-withdrawing abilities of the substituents increased, the molecular structures of the three semiconductors showed a progressive deterioration in intermolecular interactions and molecular accumulation, and the photoelectric properties became worse. Interestingly, the energy levels of the three semiconductors showed gradually decreasing changes with an enhancement of the electron-withdrawing abilities of the substituents, indicating a possible strategy for fabricating n-type anthracene derivative semiconductor materials.

Received 11th December 2020,
Accepted 21st February 2021

DOI: 10.1039/d0tc05824f

rsc.li/materials-c

Introduction

Organic semiconductor materials, which are mainly applied in the fields of organic solar cells (OSCs),^{1–3} organic field effect transistors (OFETs),^{4–6} and organic light-emitting diodes (OLEDs),^{7–9} have attracted considerable attention.¹⁰ Among the diverse organic semiconductor materials reported to date, anthracene is a hot topic that has been continuously researched and modified by scientists since it was first reported as an organic semiconductor to study electrical conductivity in 1953.^{11–13} On the one hand, the characteristics of the high fluorescence quantum efficiency makes anthracene a promising building block for use in OLEDs.^{14–16} On the other hand, the conjugated and rigid structure of anthracene provides it with charge transport properties suitable for application in field effect transistors. However, the small π -conjugation of anthracene results in a poor field-effect behavior, resulting in only $0.02 \text{ cm}^2 \text{ V}^{-1} \text{ s}^{-1}$ of the field-effect mobility.¹⁷ Therefore, researchers have introduced

some substituents to the anthracene core in order to extend the π -conjugation system and modulate the molecular packing to improve the charge transport properties.¹⁸ To date, a variety of anthracene derivatives have been designed and developed for high-performance field effect transistors.^{19–25} The 2- or 2,6-position anthracene derivatives are considered to be the most promising materials for use in anthracene derivative semiconductors and have achieved remarkable results owing to the effective molecular conjugation and molecular packing. For example, the famous molecule modified using phenyl, known as 2,6-diphenyl anthracene (2,6-DPA), possesses a hole mobility that can reach $34 \text{ cm}^2 \text{ V}^{-1} \text{ s}^{-1}$ as a result of the short-range molecular distance (2.85 \AA) and the dense molecular packing.²⁰ Li and co-workers designed and synthesized 2-naphthyl anthracene (NaAnt), the structure of which is almost planar with a small torsion angle of 0.53° between the naphthalene ring and the anthracene skeleton, and found that it exhibits a maximum mobility of $1.1 \text{ cm}^2 \text{ V}^{-1} \text{ s}^{-1}$ and a high fluorescent quantum efficiency of 40.3% in the solid state.²¹ In addition to extending the π -conjugation and improving the molecular packing, the introduction of substituents can also regulate energy levels. To date, most studies have focused on introducing electron-donating substituents (thienyl, phenyl, naphthyl, etc.) into the anthracene skeleton to realize the functionalization of novel anthracene derivatives. However, there are few studies and reports on the use of electron withdrawing groups to modify anthracene towards expected n-type molecules. Therefore, it is necessary to investigate the effect of the molecular stacking and photoelectric properties using electron withdrawing groups on the anthracene

^a Tianjin Key Laboratory of Molecular Optoelectronic Sciences, Tianjin University, Tianjin 300072, China. E-mail: zhangxt@tju.edu.cn

^b Joint School of National University of Singapore and Tianjin University, International Campus of Tianjin University, Binhai New City, Fuzhou 350207, China

† Electronic supplementary information (ESI) available: Crystallographic information for TZ-Ant and F₅Ph-Ant; transfer characteristics of FETs based on Ph-Ant and TZ-Ant; AFM characterization of Ph-Ant and TZ-Ant thin films; and CIF files for TZ-Ant and F₅Ph-Ant. CCDC 2033809 and 2033782. For ESI and crystallographic data in CIF or other electronic format see DOI: 10.1039/d0tc05824f

‡ The authors contributed equally to this work.

skeleton in order to further understand the structure–property–mobility relationship.

In this paper, the effect of three electron-withdrawing substituents on the molecular packing structure and photoelectric properties of the anthracene core are systematically studied, these are called 2-phenyl anthracene (Ph-Ant), 2-thiazole anthracene (TZ-Ant) and 2-pentafluorophenyl anthracene (F₅Ph-Ant). With the enhancement of the electron-withdrawing ability in these substituents (phenyl < thiazolyl < pentafluorophenyl), the energy levels of the semiconductors show a gradually decreasing trend which may indicate a feasible strategy to fabricate n-type materials. Moreover, the intermolecular interaction becomes weaker and the molecular accumulation becomes more loose, owing to the increasing effect of the electron-withdrawing ability. The evolution of the three molecular structures is based on classic herringbone packing (Ph-Ant), changing to herringbone packing with a slight slip (TZ-Ant), and then to a similar “face to face” stacking (F₅Ph-Ant). The field-effect mobility of the three materials are 0.2 cm² V⁻¹ s⁻¹ (Ph-Ant), 0.05 cm² V⁻¹ s⁻¹ (TZ-Ant) and 0 cm² V⁻¹ s⁻¹ (F₅Ph-Ant), respectively, which is consistent with the results of their molecular structures and the theoretical calculations. Clearly, our work may provide some useful guidance for revealing the roles of the electron-withdrawing substituents in the design and synthesis of anthracene derivative semiconductors.

Experimental

General method

All reagents and chemicals were received from commercial resources and used directly without further purification. Bruker 400 and 600 NMR spectrometer were used to record the ¹H, ¹³C and ¹⁹F NMR spectra. The deuterated reagents used for Ph-Ant and TZ-Ant were CDCl₃ with TMS (δ 0.00 ppm). F₅Ph-Ant was placed in DMSO-D₆ with TMS (δ 0.00 ppm). Thermal gravimetric analysis curves (TGA) were obtained on a METTLER TOLEDO TGA2 apparatus with a heating rate of 10 °C min⁻¹ in nitrogen. Ultraviolet-visible (UV-Vis) spectra were measured on a SHIMADZU UV-3600 UV-Vis-NIR spectrophotometer (Japan). Photoluminescence (PL) spectra were recorded on a HITACHI F-7000 spectrofluorometer (Japan). Fluorescence quantum yield was measured using an Edinburgh Instruments FLS 1000 spectrometer. Cyclic voltammetry (CV) curves were scanned on a CHI660C electrochemistry station in dry CH₂Cl₂, tetrabutylammonium hexafluorophosphate (Bu₄NPF₆) was used as an electrolyte (0.1M) and ferrocene was used as an internal standard. Glassy carbon, Pt wire and Ag/AgCl were used as the working, counter, and reference electrodes, respectively. The highest occupied molecular orbital (HOMO) energy levels were estimated according to the onsets of the oxidative peaks and the empirical formula $E_{\text{HOMO}} = -\left(E_{\text{ox}}^{\text{onset}} + 4.8 + E_{\text{Fc}/\text{Fc}^+}^{\text{onset}}\right)$ eV. The lowest unoccupied molecular orbital (LUMO) energy level was calculated by using the bandgap and the HOMO level ($E_{\text{LUMO}} = E_{\text{HOMO}} + E_{\text{g}}$). X-ray diffraction crystallography data were collected on a Rigaku Supernova CCD diffractometer with a Cu-Kα source (λ = 0.154 nm) at 293 K. The structure and refinement determinations were carried

out using Olex2 software. Atomic force microscopy (AFM) images were obtained using a Digital Instruments Nanoscope III atomic force microscope in air.

Materials

Ph-Ant was synthesized by following the procedures previously reported.²⁶ F₅Ph-Ant was synthesized as follows, to a dry 25 mL reaction flask with a stir bar, 2-bromoanthracene 100 mg (0.39 mmol), pentafluorophenylboronic acid 95.4 mg (0.45 mmol), CsF 134 mg (0.88 mmol), Ag₂O 109 mg (0.47 mmol), Pd₂(dba)₃ 18 mg (0.02 mmol) and P(*t*-Bu)₃-HBF₄ 17 mg (0.06 mmol) were added. This was then vented three times with nitrogen. Then, DMF (4 mL) that had been degassed with nitrogen was added to the reaction flask. The mixture was stirred at 100 °C for 24 h. After the reaction, the mixture was filtered through a pad of Celite, and washed with CH₂Cl₂. The filtrate was then washed with water and the organic phase was collected before being dried over anhydrous sodium sulfate and the solvent removed. After column chromatography (hexanes), 67 mg (50%) of a yellow solid was obtained. ¹H NMR (400 MHz, DMSO-d₆) δ 8.70 (d, 2H), 8.33–8.24 (m, 2H), 8.15 (d, 2H), 7.64–7.54 (m, 3H). ¹⁹F NMR (376 MHz, DMSO-d₆) δ -143.17 (dd, *J* = 24.6, 7.8 Hz, 2F), -155.88 (d, *J* = 21.9 Hz, 1F), -162.54 (dd, *J* = 22.8, 7.4 Hz, 2F). MS (EI) *m/z*: 344 [M⁺].

TZ-Ant was synthesized in two steps: (i) 2-anthraceneborate was prepared according to previously reported literature procedure.²⁷ (ii) To a dry 50 mL reaction flask with a stir bar, 2-bromo-1,3-thiazole 100 mg (0.61 mmol), 2-anthraceneborate 155 mg (0.51 mmol), K₂CO₃ 211 mg (1.53 mmol), and Pd(dppf)Cl₂ 37 mg (0.05 mmol) were added, this was then vented three times with nitrogen. Then, 1,4-dioxane (4 mL) and H₂O (2 mL), which had been degassed with nitrogen, were added to the reaction flask. The mixture was stirred at 100 °C for 16 h. After the reaction, the mixture was filtered through a pad of Celite, and washed with CH₂Cl₂. The filtrate was then washed with water and the organic phase was collected, it was then dried over anhydrous sodium sulfate and the solvent was removed. After column chromatography (hexanes), 103 mg (77%) of a yellow solid was obtained. ¹H NMR (600 MHz, CDCl₃) δ 8.63 (s, 1H), 8.52 (s, 1H), 8.43 (s, 1H), 8.08 (d, 2H), 8.04–7.99 (m, 2H), 7.95 (d, 1H), 7.53–7.47 (m, 2H), 7.40 (d, 1H). ¹³C NMR (101 MHz, CDCl₃) δ 168.65, 144.03, 132.53, 132.38, 131.89, 131.32, 130.53, 129.25, 128.40, 128.37, 127.56, 126.48, 126.48, 126.14, 125.97, 123.77, 119.11. HRMS: [M + H]⁺ = 262.0677 (calcd 262.0685).

Fabrication of the devices

A two-zone horizontal tube furnace was employed for physical vapor deposition (PVT), and the system was evacuated using a mechanical pump, which was kept at 17 Pa. The quartz boat with the Ph-Ant, TZ-Ant or F₅Ph-Ant powder of the raw materials was placed in the high-temperature zone (100, 95 and 90 °C) for 2.5 h. High-purity argon was used as the carrier gas (20 sccm). For the fabrication of the organic single crystal field effect transistors (OSCs-FETs): first, the organic semiconductor micro-nano crystals were grown on an octadecyltrichlorosilane-treated (OTS) SiO₂ (300 nm)/Si substrate using the PVT method. Then, the source electrode and drain electrode were applied by

using the “gold-layer sticking” technique.²⁸ For fabrication of the organic thin film transistor (OTFTs): thin films of the organic semiconductor were grown that were about 40 nm in thickness using vacuum deposition at a deposition speed of 0.1–0.5 Å s⁻¹ on OTS modified SiO₂/Si substrates. The field-effect transistor characteristic measurements were carried out under ambient conditions on a Keithley 4200 SCS and Micromanipulator 6150 probe station (USA). The mobility was extracted from the saturation region by using the equation $I_{DS} = (W/2L)C_{it}\mu(V_G - V_T)^2$.

Results and discussion

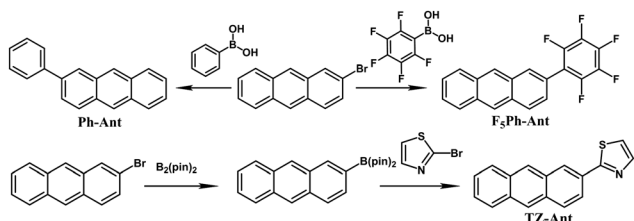
Synthesis

The target compounds (Ph-Ant, TZ-Ant, and F₅Ph-Ant) were prepared using the Suzuki coupling reaction. The synthetic routes are shown in Scheme 1. A commercially available material, 2-bromoanthracene, was used as the raw material for all reactions. 2-Anthraceneborate was synthesized according to the reported literature procedure.²⁷ The yields of Ph-Ant and TZ-Ant can reach above 70%. For F₅Ph-Ant, pentafluorophenylboronic acid (C₆F₅B(OH)₂) is a highly electron-deficient arylboronic acid, but the yield can reach 50% through the improved reaction conditions mentioned in the literature.²⁹ All products are yellow solids and were characterized using NMR and mass spectrometry.

Thermal, optical, and electrochemical properties

In a nitrogen flow, the TGA curves were measured to investigate the thermal stabilities of the three compounds, as shown in Fig. 1a. The decomposition temperatures (T_d , 5% weight loss) of Ph-Ant, TZ-Ant, and F₅Ph-Ant are 248, 240 and 214 °C. The decomposition temperature of all compounds is above 200 °C, indicating their high thermal stability.

The optical properties of the three compounds were studied using UV-Vis absorption spectroscopy and fluorescence emission spectroscopy in a dilute solution of CH₂Cl₂ (10⁻⁵ M) and the crystal powder state. The resulting spectra are shown in Fig. 1b–e and the corresponding values are listed in Table 1. The maximum absorption peaks of Ph-Ant, TZ-Ant and F₅Ph-Ant are 279, 301, and 258 nm in solution. In comparison with Ph-Ant, the absorption peaks of TZ-Ant are red-shifted; this reveals the better conjugation of the molecules when the thiazolyl group is introduced. This can also be explained by the torsion angle between the substituent and the anthracene skeleton, which is discussed in the section entitled “Crystal structure and molecular packing”. F₅Ph-Ant showed a blue-shift, fluorine atoms have more electrons than hydrogen



Scheme 1 Synthetic routes to Ph-Ant, F₅Ph-Ant, and TZ-Ant.

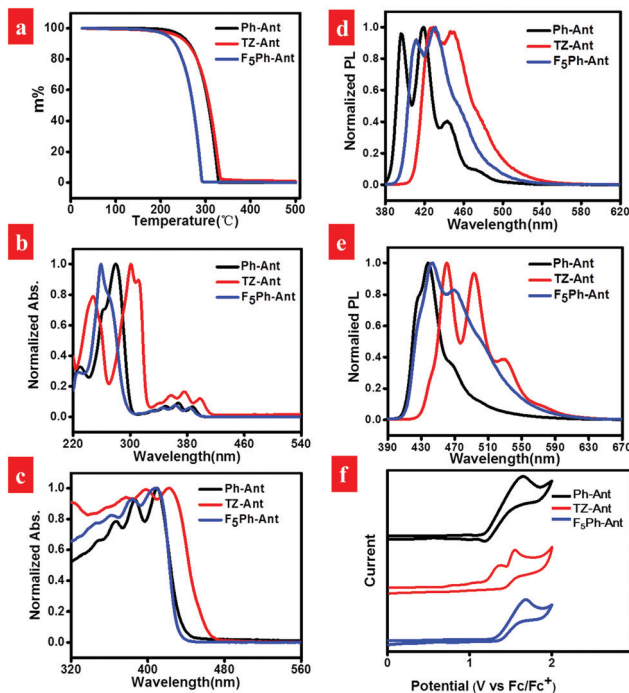


Fig. 1 (a) TGA curves of Ph-Ant, TZ-Ant, and F₅Ph-Ant. UV-vis absorption spectra of compounds in solution (b) and as solids (c). PL spectra of compounds in solution (d) and as solids (e). (f) Cyclic voltammogram curves for Ph-Ant, TZ-Ant, and F₅Ph-Ant.

Table 1 Physicochemical properties of the three materials

Compound	TGA (°C)	$\lambda_{\text{max}}^{\text{Sol}}$ (nm)	E_g (eV)	PLQY (%)
Ph-Ant	246 °C	279	2.97	28.87
TZ-Ant	241 °C	301	2.90	10.89
F ₅ Ph-Ant	215 °C	258	3.00	18.21

atoms owing to their strong electronegativity, resulting in an increase in the electrostatic repulsion and steric hindrance between the pentafluorophenyl group and the anthracene core, which reduces the degree of conjugation. This also indicates that the structural planarity of F₅Ph-Ant is not as good as that of Ph-Ant. The absorption peaks in the solid state showed a bathochromic shift, as compared to that in solution, indicating the formation of J-aggregates in the solid form. The optical energy level band gaps (E_g) of the compounds calculated from their respective initial absorption wavelengths were –2.97, –2.90, and –3.00 eV for Ph-Ant, TZ-Ant and F₅Ph-Ant. The fluorescence emission peaks range from about 400 to 540 nm, mainly showing a blue light emission with photoluminescence quantum yield (PLQY) values of 28.87%, 10.89%, and 18.21% for Ph-Ant, TZ-Ant, and F₅Ph-Ant in the solid state.

Cyclic voltammetry (CV) measurements in dry dichloromethane (CH₂Cl₂) were performed to explore the electrochemical properties and oxidative stability of these compounds, as shown in Fig. 1f. Using ferrocene as the internal standard, the HOMO levels for compounds Ph-Ant, TZ-Ant, F₅Ph-Ant were respectively calculated

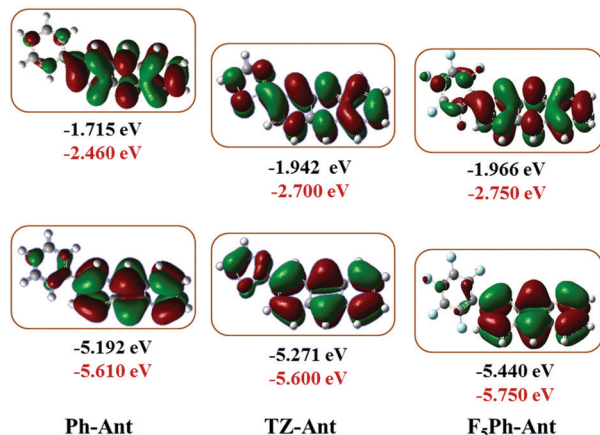


Fig. 2 The frontier molecular orbitals calculated using DFT theory and the energy levels calculated using theoretical (black) and experimental tests (red).

to be -5.61 , -5.60 , and -5.75 eV according to the onset of the oxidation peaks. The LUMO energy levels for the anthracene derivatives were Ph-Ant: -2.64 eV, TZ-Ant: -2.70 eV, and F₅Ph-Ant: -2.75 eV, which were calculated from the band gap and the HOMO energy level ($E_{\text{LUMO}} = E_{\text{HOMO}} + E_g$). These values indicate that the materials have a good ambient stability, which is consistent with the wide band gaps. Compared with the other two anthracene derivatives, F₅Ph-Ant has the deepest HOMO level owing to the strong electron-withdrawing ability of the substituents. Thiazolyl is a weaker electron-withdrawing group, and the LUMO energy level of TZ-Ant also showed a decrease. In addition, the frontier molecular orbitals and energy levels of the three compounds were calculated using density functional theory (DFT) calculations, see Fig. 2. The energy levels calculated using DFT were -5.192 , -5.271 , and -5.440 eV (HOMO) and -1.715 , -1.942 , and -1.966 eV (LUMO) for Ph-Ant, TZ-Ant, and F₅Ph-Ant. Showing a slight decreasing trend, which is in line with that obtained using cyclic voltammetry. The energy levels of the three materials did not achieve a low LUMO energy level (-3 to -4.5 eV) for the n-type semiconductor materials, but the energy levels gradually decreased with the enhancement of the electron withdrawing ability of the substituents, indicating that this strategy is feasible.

Crystal structure and molecular packing

The crystal structure and molecular packing of the three materials were analyzed and compared to study the influence of the substituents on the structure. High-quality single crystals of TZ-Ant and F₅Ph-Ant were grown by slowly volatilizing the saturated ethyl acetate solution of TZ-Ant and the saturated petroleum ether solution of F₅Ph-Ant for X-ray diffraction analysis (TZ-Ant, CCDC: 2033809; F₅Ph-Ant, CCDC: 2033782). The crystal data for Ph-Ant (CCDC: 1435446) were obtained from the literature.³⁰ The crystallographic data for TZ-Ant and F₅Ph-Ant are presented in Table S1 (ESI[†]). The crystal structure and molecular packing of Ph-Ant, TZ-Ant, and F₅Ph-Ant are shown in Fig. 3. Fig. 3a and b shows that Ph-Ant molecules have

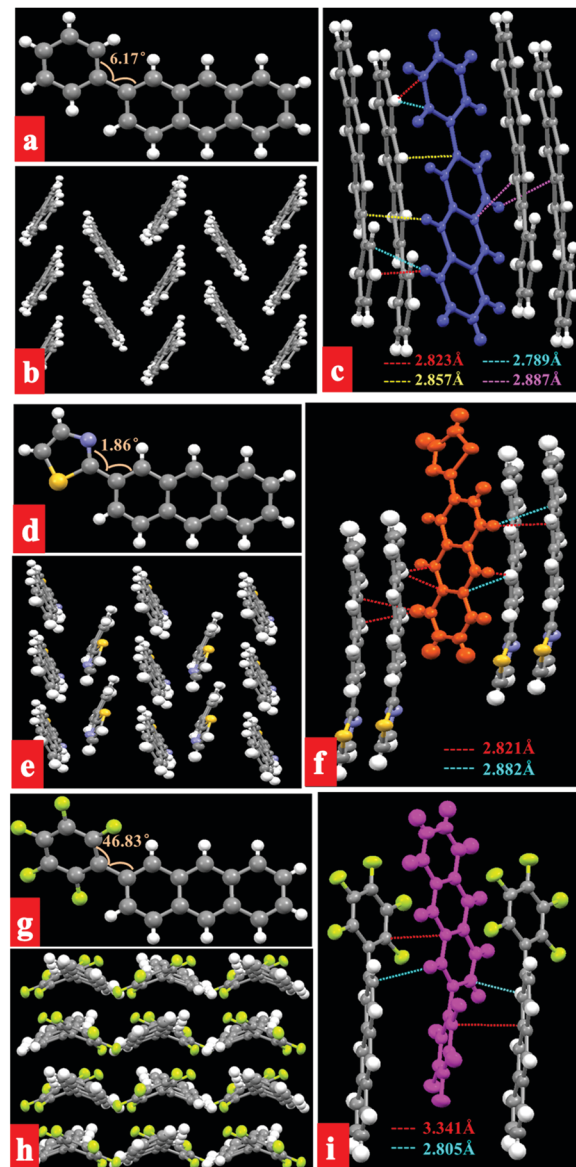


Fig. 3 Single-crystal structures, packing motifs, and short contacts for Ph-Ant (a–c), TZ-Ant (d–f), and F₅Ph-Ant (g–i).

a torsion angle of 6.17° between the benzene ring and the anthracene core and are packed in a typical herringbone arrangement. Multiple C–H \cdots π interactions with distances between 2.339 – 2.868 Å are observed for each Ph-Ant molecule with its four neighboring molecules (Fig. 3c). The information indicates that it has good charge transport properties.^{20–23} For TZ-Ant, the crystal system is orthorhombic and the space group is *Pna*2₁. As shown in Fig. 3d, the TZ-Ant molecule is almost flat with a small torsion of 1.86° between the substituent and the anthracene skeleton, which indicates that it has a better planarity than Ph-Ant and corresponds to the ultraviolet absorption red-shift mentioned above. The central molecule interacts with four adjacent molecules, two types of C–H \cdots π interactions are observed at distances of 2.821 and 2.882 Å, see Fig. 3f. TZ-Ant adopts a herringbone stacking mode (Fig. 3e),

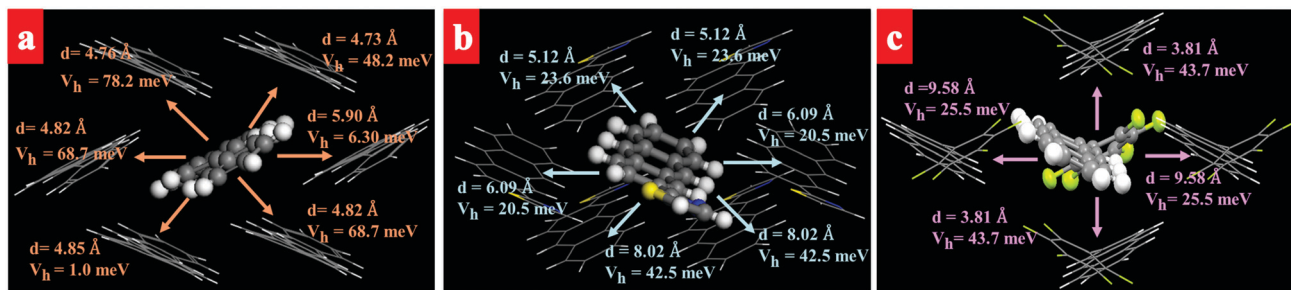


Fig. 4 Illustrations of the charge transport pathways and transport integrals of the holes and the intermolecular distances between the two parallel planes of (a) Ph-Ant, (b) TZ-Ant, and (c) F₅Ph-Ant.

which is different from that of Ph-Ant; there is a slip along the long axis between the central molecule and the neighboring molecules (Fig. S1d, ESI[†]), which reduces the “edge-to-face” overlap and adversely effects the charge transfer properties.³¹ The X-ray crystallographic results show that F₅Ph-Ant belongs to the orthorhombic *Pna2*₁ space group. A similar accumulation of “face to face” was observed, see Fig. 3h and Fig. S1 (ESI[†]). However, there is a large torsion angle of 46.83° (Fig. 3g) between the pentafluorophenyl group and the anthracene core in F₅Ph-Ant, therefore the molecular planarity and π -conjugation are far less than that of Ph-Ant and TZ-Ant. The large twist angle not only effects the planarity of the molecules, but also causes the molecular packing to appear looser and the intermolecular interaction to decrease. As shown in Fig. 3i, F₅Ph-Ant only interacts with two surrounding molecules with a C–H– π interaction distance of 2.805 Å and a C–C interaction distance of 3.341 Å. The loose accumulation of molecules may have negative effects. Based on the Gaussian software suite at the B3LYP/6-31G(d)/LANL2DZ level of theory, the values of the hole (V_h) transport integrals and intermolecular distances between the two parallel planes of three materials are shown in Fig. 4. The decreasing V_h are consistent with the deteriorative molecular structures.

Charge transport properties of OFETs

Bottom-gate top-contact OFETs (Fig. 5a and Fig. S3a, ESI[†]) based on the above three semiconductors were fabricated to study the charge transport properties. The thin-film-based OFETs based on Ph-Ant and TZ-Ant exhibited a typical p-type mobility of 0.087 and $7 \times 10^{-5} \text{ cm}^2 \text{ V}^{-1} \text{ s}^{-1}$, respectively, as shown in Fig. S2 (ESI[†]). To further determine the intrinsic charge transport efficiency of semiconductors, single-crystal-based OFETs were successfully constructed onto the OTS modified SiO₂/Si substrates by using the “gold-layer sticking” technique.

Fig. 5b and c shows the mobility of Ph-Ant reached $0.2 \text{ cm}^2 \text{ V}^{-1} \text{ s}^{-1}$ with a current on/off ratio of 10^6 . For the TZ-Ant device, a lower mobility of $0.005 \text{ cm}^2 \text{ V}^{-1} \text{ s}^{-1}$ with a current on/off ratio of 10^5 was obtained, and the transfer curve is shown in Fig. S3b (ESI[†]). In contrast, the decreasing mobility of the TZ-Ant device is caused by the deteriorative crystal structure and packing, compared to that of Ph-Ant. In our study, the F₅Ph-Ant devices do not show normal field-effect properties, this may be due to the poor molecular planarity, unsatisfactory molecular stacking and weak molecular interaction caused by the large torsion angle. Clearly, the field-effect mobility based on thin films and the single crystals all showed decreasing variation trends with the increasing electron-withdrawing ability in the asymmetric anthracene derivative semiconductors with different electron withdrawing substituents (Fig. 5d).

Conclusions

In summary, three 2-substituted anthracene derivatives were synthesized that were modified with three different electron-withdrawing substituents: TZ-Ant, Ph-Ant, and F₅Ph-Ant. It was found that the quality of the molecular packing structures of the anthracene derivatives and the photoelectric properties were significantly decreased with an increase in the electron-withdrawing abilities. Interestingly, the energy levels of the three compounds also showed a decreasing trend with an increase in the electron-withdrawing abilities, which may provide useful guidance for the design and synthesis of n-type anthracene derivative semiconductors. In addition, single-crystal-based OFETs were successfully constructed to further reveal the intrinsic electrical properties of the above three materials, the mobility of which

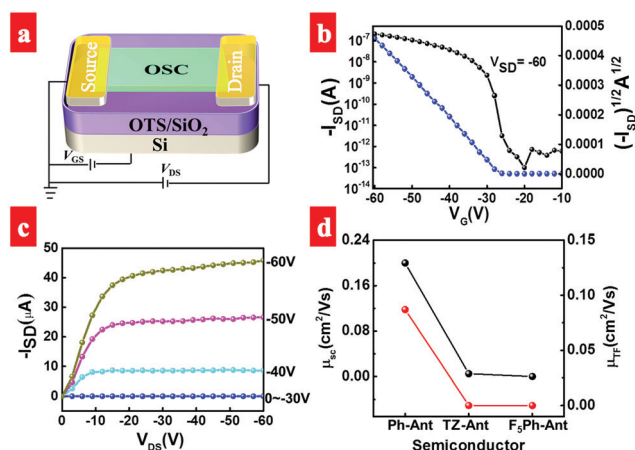


Fig. 5 (a) A schematic diagram of the OSC-FET. (b) Typical transfer and (c) output curves of the single-crystal-based transistor of Ph-Ant. (d) Mobilities of the three materials based on single-crystal (black) and thin-film (red) field-effect transistors.

decreased from $0.2 \text{ cm}^2 \text{ V}^{-1} \text{ s}^{-1}$ to 0, which was consistent with the results obtained from their molecular structures and theoretical calculations.

Conflicts of interest

There are no conflicts of interest to declare.

Acknowledgements

The authors acknowledge financial support from the National Key R&D Program (2017YFA0204503), and the National Natural Science Foundation of China (91833306, 21875158, 51633006, and 51733004).

Notes and references

- 1 T. Zhang and R. J. Holmes, *Appl. Phys. Lett.*, 2018, **113**, 143302.
- 2 Y. Yao, L. Zhang, T. Leydecker and P. Samori, *J. Am. Chem. Soc.*, 2018, **140**, 6984–6990.
- 3 X. Zhang, H. Dong and W. Hu, *Adv. Mater.*, 2018, **30**, 1801048.
- 4 Y. Yao, Y. Chen, H. Wang and P. Samori, *SmartMat*, 2020, **1**, e1009.
- 5 J. Mei, Y. Diao, A. L. Appleton, L. Fang and Z. Bao, *J. Am. Chem. Soc.*, 2013, **135**, 6724–6746.
- 6 X. Zhang, G. Zhao, Y. Zhen, Z. Tu, P. He, Y. Yi, H. Dong and W. Hu, *J. Mater. Chem. C*, 2015, **3**, 5368–5371.
- 7 Shahnawaz, S. S. Swayamprabha, M. R. Nagar, R. A. K. Yadav, S. Gull, D. K. Dubey and J.-H. Jou, *J. Mater. Chem. C*, 2020, **8**, 10464.
- 8 H. Zhu, E.-S. Shin, A. Liu, D. Ji, Y. Xu and Y.-Y. Noh, *Adv. Funct. Mater.*, 2019, 1904588.
- 9 S. Engmann, A. J. Barito, E. G. Bittle, N. C. Giebink, L. J. Richter and D. J. Gundlach, *Nat. Commun.*, 2019, **10**, 227.
- 10 C. Wang, H. Dong, L. Jiang and W. Hu, *Chem. Soc. Rev.*, 2018, **47**, 422–500.
- 11 H. Mette and H. Pick, *Z. Phys.*, 1953, **134**, 566–575.
- 12 J. Van Damme and F. Du Prez, *Prog. Polym. Sci.*, 2018, **82**, 92–119.
- 13 C. Wang, H. Dong, W. Hu, Y. Liu and D. Zhu, *Chem. Rev.*, 2012, **112**, 2208–2267.
- 14 J. Liu, L. Meng, W. Zhu, C. Zhang, H. Zhang, Y. Yao, Z. Wang, P. He, X. Zhang and Y. Wang, *J. Mater. Chem. C*, 2015, **3**, 3068–3071.
- 15 M. Chen, Y. Zhao, L. Yan, S. Yang, Y. Zhu, I. Murtaza, G. He, H. Meng and W. Huang, *Angew. Chem., Int. Ed.*, 2017, **56**, 722–727.
- 16 J. Zhang, B. Xu, J. Chen, S. Ma, Y. Dong, L. Wang, B. Li, L. Ye and W. Tian, *Adv. Mater.*, 2014, **26**, 739–745.
- 17 A. N. Aleshin, J. Y. Lee, S. W. Chu, J. S. Kim and Y. W. Park, *Appl. Phys. Lett.*, 2004, **84**, 5383–5385.
- 18 M. Chen, L. Yan, Y. Zhao, I. Murtaza, H. Meng and W. Huang, *J. Mater. Chem. C*, 2018, **6**, 7416–7444.
- 19 A. Dadvand, A. G. Moiseev, K. Sawabe, W. Sun, B. Djukic, I. Chung, T. Takenobu, F. Rosei and D. F. Perepichka, *Angew. Chem., Int. Ed.*, 2012, **51**, 3837–3841.
- 20 J. Liu, H. Zhang, H. Dong, L. Meng, L. Jiang, L. Jiang, Y. Wang, J. Yu, Y. Sun, W. Hu and A. J. Heeger, *Nat. Commun.*, 2015, **6**, 10032.
- 21 J. Li, J. Liu, Y. Zhen, L. Meng, Y. Wang, H. Dong and W. Hu, *J. Mater. Chem. C*, 2015, **3**, 10695–10698.
- 22 J. Li, K. Zhou, J. Liu, Y. Zhen, L. Liu, J. Zhang, H. Dong, X. Zhang, L. Jiang and W. Hu, *J. Am. Chem. Soc.*, 2017, **139**, 17261–17264.
- 23 J. Liu, H. Dong, Z. Wang, D. Ji, C. Cheng, H. Geng, H. Zhang, Y. Zhen, L. Jiang, H. Fu, Z. Bo, W. Chen, Z. Shuai and W. Hu, *Chem. Commun.*, 2015, **51**, 11777–11779.
- 24 Y. Chen, C. Li, X. Xu, M. Liu, Y. He, I. Murtaza, D. Zhang, C. Yao, Y. Wang and H. Meng, *ACS Appl. Mater. Interfaces*, 2017, **9**, 7305–7314.
- 25 L. Yan, Y. Zhao, H. Yu, Z. Hu, Y. He, A. Li, O. Goto, C. Yan, T. Chen, R. Chen, Y.-L. Loo, D. F. Perepichka, H. Meng and W. Huang, *J. Mater. Chem. C*, 2016, **4**, 3517–3522.
- 26 C. Xu, P. He, J. Liu, A. Cui, H. Dong, Y. Zhen, W. Chen and W. Hu, *Angew. Chem., Int. Ed.*, 2016, **55**, 9519–9523.
- 27 K. Ito, T. Suzuki, Y. Sakamoto, D. Kubota, Y. Inoue, F. Sato and S. Tokito, *Angew. Chem., Int. Ed.*, 2003, **42**, 1159–1162.
- 28 Q. Tang, L. Jiang, Y. Tong, H. Li, Y. Liu, Z. Wang, W. Hu, Y. Liu and D. Zhu, *Adv. Mater.*, 2008, **20**, 2947–2951.
- 29 T. Korenaga, T. Kosaki, R. Fukumura, T. Ema and T. Sakai, *Org. Lett.*, 2005, **7**, 4915–4917.
- 30 H. L. van de Wouw, J. Y. Lee, M. A. Siegler and R. S. Klausen, *Org. Biomol. Chem.*, 2016, **14**, 3256–3263.
- 31 J. Liu, W. Zhu, K. Zhou, Z. Wang, Y. Zou, Q. Meng, J. Li, Y. Zhen and W. Hu, *J. Mater. Chem. C*, 2016, **4**, 3621–3627.